

GPU acceleration of many-body perturbation theory methods in MOLGW with OpenACC

Young-Moo Byun¹ and Jejoong Yoo^{1,*}

¹*Department of Physics, Sungkyunkwan University, Suwon-si, Gyeonggi-do 16419, Korea*

(Dated: December 5, 2023)

Quasiparticle self-consistent many-body perturbation theory (MBPT) methods that update both eigenvalues and eigenvectors can calculate the excited-state properties of molecular systems without depending on the choice of starting points. However, those methods are computationally intensive even on modern multi-core central processing units (CPUs) and thus typically limited to small systems. Many-core accelerators such as graphics processing units (GPUs) may be able to boost the performance of those methods without losing accuracy, making starting-point-independent MBPT methods applicable to large systems. Here, we GPU accelerate MOLGW, a Gaussian-based MBPT code for molecules, with open accelerators (OpenACC) and achieve speedups of up to 9.7x over 32 open multi-processing (OpenMP) CPU threads.

I. INTRODUCTION

A theoretical method capable of accurately and efficiently describing the excited-state properties of molecular systems is important for the rational design of molecules with desired properties. Many-body perturbation theory (MBPT) methods based on the one-body Green's function G might be a good choice, because the GW method with W being the dynamically screened Coulomb interaction has been successfully used to calculate electronic excitations in solids for a few decades.¹ For example, the non-self-consistent (one-shot) GW method (G_0W_0) starting from the Perdew–Burke–Ernzerhof (PBE) generalized gradient approximation to density-functional theory ($G_0W_0@PBE$ using the {MBPT method}@{starting point} notation) can accurately calculate the bandgap of semiconductors at a reasonably low computational cost.^{2,3}

However, $G_0W_0@PBE$ fails for molecules, significantly underestimating the ionization energy (IE) of small sp and $3d$ molecules by ~ 0.5 and ~ 1.0 eV, respectively.^{4,5} A simple workaround to make the G_0W_0 method work for finite systems is to change its starting point from the PBE exchange-correlation functional to the Hartree–Fock (HF) exchange or hybrid functionals, which admix a fraction of non-local HF (exact) exchange with semilocal exchange.⁶ However, this workaround makes the G_0W_0 method *empirical*; G_0W_0 is system dependent and its results depend strongly on the choice of starting points.^{5,7} The quasiparticle self-consistent GW (qs GW) method can address the system and starting-point dependency issues of the G_0W_0 method,^{8–10} giving good results for both the bandgap of solids and the IE of atoms and molecules.^{7,11–15} However, the qs GW method is computationally expensive even for small systems, making qs GW calculations of large systems not feasible even on high-performance computing (HPC) supercomputers powered by modern multi-core central processing units (CPUs).

Graphics processing units (GPUs) may solve the efficiency problem of the qs GW method, enabling large-

scale qs GW calculations without compromising accuracy.^{16–18} GPUs were accelerators (special-purpose hardware) designed for computer graphics at first, but later general-purpose computing on graphics processing units (GPGPU) made it possible for GPUs to perform non-specialized computations that have typically been conducted by CPUs. On the hardware side, GPUs consisting of many lightweight cores can accelerate numerically intensive and massively parallel computations in a single instruction multiple threads (SIMT) fashion. Some modern GPUs supporting high-performance double-precision floating-point (FP64) computations are widely used for HPC scientific applications that require high precision and accuracy for reliability and stability, such as *ab initio* quantum chemistry applications.^{19–26}

On the software side, there are two popular and mature GPU programming models: compute unified device architecture (CUDA) and open accelerators (OpenACC). While CUDA is a low-level model and is an extension to C/C++/Fortran,²⁷ like open multi-processing (OpenMP), OpenACC is a high-level model based on compiler directives.²⁸ CUDA enables to harness the parallel computing power of GPUs, but CUDA programming could be complex, because it requires an understanding of the GPU hardware architecture and a significant modification of the original CPU source code. Also, the CUDA code runs only on NVIDIA GPUs. OpenACC is an alternative to CUDA to simplify parallel programming and make the parallel code portable across various kinds of platforms such as operating systems, compilers, CPUs, and GPUs.

As the creator of the Python programming language said “Maintainable code is more important than clever code,”²⁹ maintainability is as important as performance in software development, including the development of HPC scientific applications. OpenACC achieves a balance between productivity and performance by enabling scientists and researchers to accelerate existing CPU codes on GPUs quickly with minimal programming effort, and thus is becoming increasingly popular.^{30–34} For example, the GPU port of VASP has lately transitioned

from CUDA to OpenACC, because ‘‘OpenACC dramatically decreases GPU development and maintenance efforts.’’^{35,36}

In recent years, MBPT methods for molecules with local orbitals have been implemented in a variety of electronic structure codes, including FIESTA,³⁷ FHI-AIMS,³⁸ TURBOMOLE,³⁹ CP2K,⁴⁰ and MOLGW.⁴¹ Among those codes, MOLGW is a double-precision Fortran/C++/Python CPU code for MBPT excited-state calculations of molecular systems based on Gaussian basis sets. Although one of us has recently parallelized MOLGW with OpenMP, starting-point-independent MBPT methods, such as qsGW, in OpenMP-parallelized MOLGW still are too time-consuming to be applied to large systems.^{5,7}

In this work, we port MOLGW to the GPU using OpenACC to extend the range of its applicability while keeping the original CPU source code intact. We benchmark the performance of GPU-enabled MOLGW and find that the OpenACC version of MOLGW on desktop GPUs can outperform the OpenMP version on workstation and supercomputer CPUs.

The rest of this paper is structured as follows: First, we give a mathematical introduction to MBPT. Second, we overview our OpenACC implementation of MBPT methods in MOLGW. Third, we analyze and discuss our benchmark results for the performance of our GPU-accelerated MOLGW. Last, we summarize and conclude.

II. THEORETICAL BACKGROUND

In this section, we give a minimal and simplified introduction to MBPT related to OpenMP and OpenACC implementations in MOLGW. More details about MBPT can be found elsewhere.^{7,11,38,42,43} We use a simple and consistent notation: (i) we follow the notations in MOLGW implementation and application papers,^{5,7,41} (ii) we use Hartree atomic units, and (iii) we omit the complex conjugate notation, because we consider real wavefunctions.

A. Many-body perturbation theory (MBPT)

MBPT can be used to calculate electron addition and removal energies. In MBPT, the central quantity is the one-body Green’s function:

$$G^\sigma(\mathbf{r}, \mathbf{r}', \omega) = \sum_i \frac{\varphi_i^\sigma(\mathbf{r})\varphi_i^\sigma(\mathbf{r}')}{\omega - \epsilon_i^\sigma - i\eta} + \sum_a \frac{\varphi_a^\sigma(\mathbf{r})\varphi_a^\sigma(\mathbf{r}')}{\omega - \epsilon_a^\sigma + i\eta}, \quad (1)$$

where σ is the spin direction, ω is frequency (energy), η is a positive infinitesimal, ϵ_m^σ and φ_m^σ are one-electron energies and wavefunctions, respectively, and i and a run over occupied and empty (unoccupied or virtual) states, respectively. In the following, we omit space and frequency variables ($\mathbf{r}, \mathbf{r}', \omega$) for notational simplicity whenever needed.

Once the non-interacting (bare) Green’s function G_0^σ is known, the interacting (dressed) Green’s function G^σ can be obtained by solving the Dyson equation:

$$G^\sigma = G_0^\sigma + G_0^\sigma \Delta \Sigma^\sigma G^\sigma, \quad (2)$$

where Σ^σ is the non-local, frequency-dependent (dynamical), and non-Hermitian self-energy, which accounts for many-body effects. Two popular approximations to the self-energy are the *GW* approximation and second-order Møller-Plesset perturbation theory (MP2), which are based on W and the bare (unscreened) Coulomb interaction v , respectively.^{38,43}

B. Self-consistent field (SCF)

In MBPT for molecules using localized orbitals, the molecular orbitals (MOs) and MO energies are used as one-electron wavefunctions and energies, respectively, to construct the Green’s function in Eq. (1). MOs can be expressed as a linear combination of atomic orbitals ϕ_μ (LCAO):

$$\varphi_m^\sigma(\mathbf{r}) = \sum_\mu C_{\mu m}^\sigma \phi_\mu(\mathbf{r}), \quad (3)$$

where $C_{\mu m}^\sigma$ are the LCAO-MO coefficients. MOLGW uses Gaussian-type orbitals (GTOs) as AOs.

The LCAO-MO coefficients in Eq. (3) can be obtained from a self-consistent solution to a generalized eigenvalue problem:

$$\mathbf{H}^\sigma \mathbf{C}^\sigma = \mathbf{S} \mathbf{C}^\sigma \epsilon^\sigma, \quad (4)$$

where \mathbf{C}^σ is a matrix of LCAO-MO coefficients, ϵ^σ is a diagonal matrix of MO energies, \mathbf{S} is the AO overlap matrix:

$$S_{\mu\nu} = \int d\mathbf{r} \phi_\mu(\mathbf{r})\phi_\nu(\mathbf{r}), \quad (5)$$

and \mathbf{H}^σ is the Hamiltonian matrix:

$$H_{\mu\nu}^\sigma = T_{\mu\nu} + V_{\text{ext},\mu\nu} + J_{\mu\nu} - K_{\mu\nu}^\sigma + \Sigma_{\text{c},\mu\nu}^\sigma, \quad (6)$$

where T , V_{ext} , J , and K^σ are the kinetic energy, external potential energy, Hartree, and Fock exchange terms, respectively, and Σ_{c}^σ is the correlation part of the self-energy. When $\Sigma_{\text{c}}^\sigma = 0$ (neglecting electron correlation effects) in Eq. (6), Eq. (4) becomes the HF equation.

We parallelize the last three terms on the right side of Eq. (6) – J , K^σ , and Σ_{c}^σ – using OpenACC in this work. The Hartree term in Eq. (6) is given by

$$J_{\mu\nu} = \sum_{\lambda\tau} (\mu\nu|\lambda\tau) \sum_\sigma D_{\lambda\tau}^\sigma, \quad (7)$$

where $(\mu\nu|\lambda\tau)$ are the 4-center two-electron Coulomb repulsion integrals:

$$(\mu\nu|\lambda\tau) = \iint d\mathbf{r}d\mathbf{r}' \phi_\mu(\mathbf{r})\phi_\nu(\mathbf{r}) \frac{1}{|\mathbf{r} - \mathbf{r}'|} \phi_\lambda(\mathbf{r}')\phi_\tau(\mathbf{r}'), \quad (8)$$

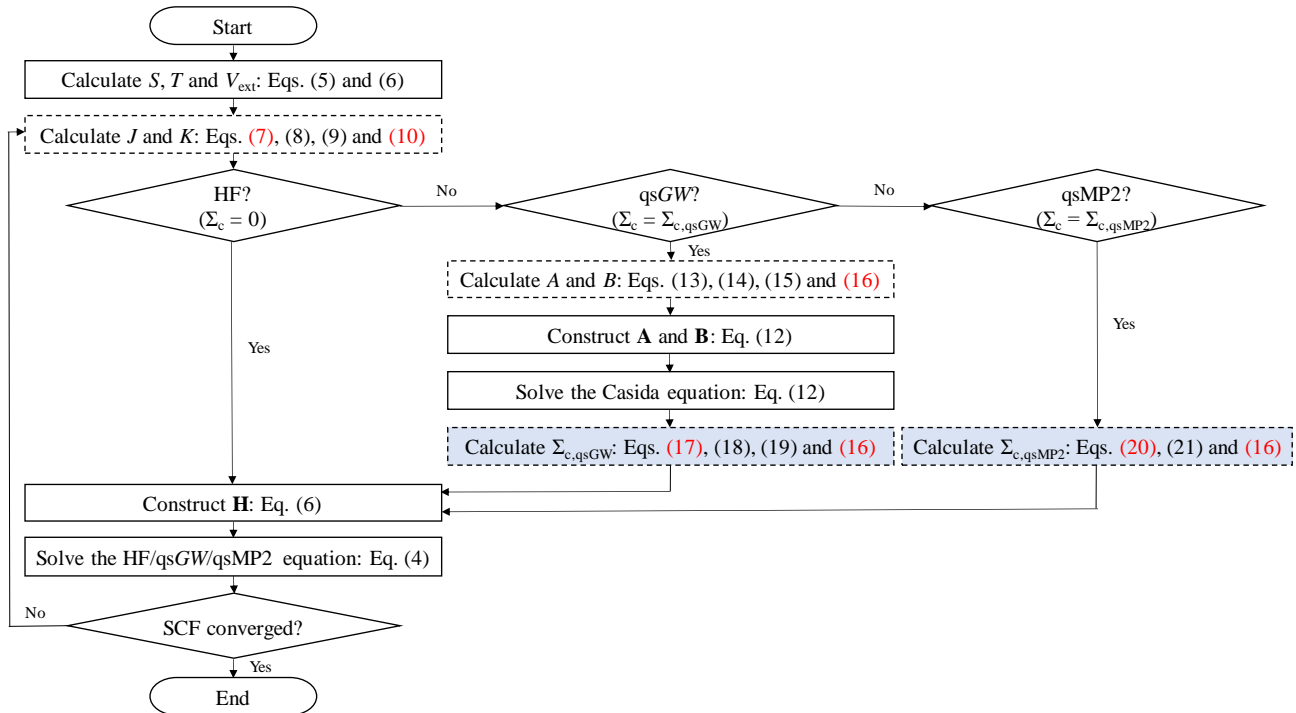


FIG. 1. (Color online) Flowchart of qsGW and qsMP2 implementations in MOLGW. Boxes with a dashed line represent computational bottlenecks in this work. Light blue boxes represent major computational bottlenecks in this work. OpenMP- and OpenACC-parallelized equations are highlighted in red.

TABLE I. OpenACC directives and clauses used in this work. N_{kernel} represents the number of kernels in a computational bottleneck. AO-MO represents the atomic orbital-to-molecular orbital integral transformation.

Bottleneck	Equations	Function/subroutine and file ^a	N_{kernel}	OpenACC directives and clauses ^b
N/A ^c	Eq. (8)	See footnote ^d m_eri.f90	N/A ^c	declare/create/update/device & routine/seq
Hartree J	Eq. (7)	setup_hartree() m_hamiltonian.f90	1	data/copyin/copy & parallel/loop/collapse/seq
Exchange K	Eq. (10)	setup_exchange() m_hamiltonian.f90	1	data/copyin/copy & parallel/loop/collapse/seq
AO-MO ^e	Eq. (16)	calculate_eri_4center_eigen() m_eri_ao_mo.f90	4	data/copyin/copyout & parallel/loop/collapse/seq
Σ_c^{qsGW} excl. AO-MO ^e	Eqs. (17), (18) & (19)	chi_to_vchiv() linear_response.f90	1	data/enter data/exit data/copyin/copyout ^f & parallel/loop/collapse
Σ_c^{qsMP2} excl. AO-MO ^e	Eqs. (20) & (21)	pt2_selfenergy_qs() pt2_selfenergy.f90	1	data/copyin/copy & parallel/loop/collapse/seq

^a Functions and subroutines are in the first line, and files are in the second line.

^b For data movement (first line) and computation (second line)

^c Not available because what OpenACC does in this Fortran module is not parallelizing computational bottlenecks, but transferring global data from CPU memory to GPU memory.

^d Functions: negligible_basispair(), index_eri(), index_pair(), and eri(). Subroutines: prepare_eri(), setup_shell_index(), setup_basispair(), and identify_negligible_shellpair().

^e These three are major computational bottlenecks in this work.

^f CUDA unified (managed) memory can optimize data transfer in this kernel.

and \mathbf{D}^σ is the density matrix:

$$D_{\mu\nu}^\sigma = \sum_m f_m^\sigma C_{\mu m}^\sigma C_{\nu m}^\sigma, \quad (9)$$

where f_m^σ are occupation numbers (0 or 1). The Fock exchange term in Eq. (6) is given by

$$K_{\mu\nu}^\sigma = \sum_{\lambda\tau} D_{\lambda\tau}^\sigma (\mu\lambda|\tau\nu). \quad (10)$$

It should be noted that the resolution-of-identity (RI) approximation (the density-fitting approximation) significantly reduces the computational and memory costs of the 4-center integrals in Eq. (8) at the cost of a slight accuracy loss.^{5,38} In MOLGW, the RI approximation is parallelized using message passing interface (MPI).⁴¹ In this work, the MPI-parallelized RI approximation in MOLGW is not ported to the GPU, because the RI-MP2 implementation in MOLGW suffers from the MPI communication overhead (the communication time is much greater than the computation time),⁷ and fixing the issue is beyond the scope of this work.

C. GW approximation

The *GW* approximation neglecting vertex corrections (electron-hole interactions) is the first-order expansion of the self-energy in W . The interacting (reducible) polarizability χ is needed to obtain the correlation part of the *GW* self-energy $\Sigma_c^{\text{GW},\sigma}$:

$$\Sigma_c^{\text{GW},\sigma} = iG^\sigma(W - v) = iG^\sigma v\chi v, \quad (11)$$

and χ within the random-phase approximation (RPA) can be obtained by solving the Casida equation:

$$\begin{pmatrix} \mathbf{A} & \mathbf{B} \\ -\mathbf{B} & -\mathbf{A} \end{pmatrix} \begin{pmatrix} X^s \\ Y^s \end{pmatrix} = \begin{pmatrix} X^s \\ Y^s \end{pmatrix} \Omega_s, \quad (12)$$

where \mathbf{A} and \mathbf{B} are the resonant and coupling matrices, respectively, and (X^s, Y^s) and Ω_s are the eigenvectors and corresponding eigenvalues, respectively. \mathbf{A} and \mathbf{B} are given by

$$A_{ia\sigma}^{jb\sigma'} = (\epsilon_a^\sigma - \epsilon_i^\sigma) \delta_{ij} \delta_{ab} \delta_{\sigma\sigma'} - (ia\sigma|jb\sigma'), \quad (13)$$

$$B_{ia\sigma}^{jb\sigma'} = -(ia\sigma|bj\sigma'), \quad (14)$$

where i and j are for occupied states, a and b are for empty states, and $(ia\sigma|jb\sigma')$ are the 4-orbital two-electron Coulomb repulsion integrals:

$$(ia\sigma|jb\sigma') = \iint d\mathbf{r}d\mathbf{r}' \varphi_i^\sigma(\mathbf{r})\varphi_a^\sigma(\mathbf{r}) \frac{1}{|\mathbf{r}-\mathbf{r}'|} \varphi_j^{\sigma'}(\mathbf{r}')\varphi_b^{\sigma'}(\mathbf{r}'), \quad (15)$$

which is obtained from the AO-MO integral transformation:

$$(ia\sigma|jb\sigma') = \sum_{\mu\nu\lambda\tau} C_{\mu i}^\sigma C_{\nu a}^\sigma C_{\lambda j}^{\sigma'} C_{\tau b}^{\sigma'} (\mu\nu|\lambda\tau). \quad (16)$$

Once (X^s, Y^s) and Ω_s in Eq. (12) are found, one can obtain the spectral (Lehmann) representation of $\chi(\omega)$, $W(\omega)$, and $\Sigma_c^{\text{GW},\sigma}(\omega)$ successively, as shown in Eq. (11). $\Sigma_c^{\text{GW},\sigma}(\omega)$ is given by

$$\begin{aligned} \langle \varphi_m^\sigma | \Sigma_c^{\text{GW},\sigma}(\omega) | \varphi_n^\sigma \rangle &= \sum_{is} \frac{w_{mi\sigma}^s w_{ni\sigma}^s}{\omega - \epsilon_i^\sigma + \Omega_s - i\eta} \\ &+ \sum_{as} \frac{w_{ma\sigma}^s w_{na\sigma}^s}{\omega - \epsilon_a^\sigma - \Omega_s + i\eta}, \end{aligned} \quad (17)$$

where i runs over occupied states, a runs over empty states, s runs over all excitations, and $w_{mn\sigma}^s$ are given by

$$w_{mn\sigma}^s = \sum_{ia\sigma'} (mn\sigma|ia\sigma') (X_{ia\sigma'}^s + Y_{ia\sigma'}^s). \quad (18)$$

The conventional G_0W_0 method uses only diagonal elements ($m = n$) of Eq. (17) for efficiency, giving only quasiparticle (QP) energies.

In order to remove the starting point dependency in the G_0W_0 method, Faleev and co-workers proposed the qs*GW* method using a static and Hermitian approximation to the *GW* self-energy.⁸⁻¹⁰ The correlation part of the ‘‘mode A’’ qs*GW* self-energy $\Sigma_c^{\text{qsGW},\sigma}$ is given by

$$\begin{aligned} \langle \varphi_m^\sigma | \Sigma_c^{\text{qsGW},\sigma} | \varphi_n^\sigma \rangle \\ = \frac{1}{2} [\langle \varphi_m^\sigma | \Sigma_c^{\text{GW},\sigma}(\epsilon_n^\sigma) | \varphi_n^\sigma \rangle + \langle \varphi_n^\sigma | \Sigma_c^{\text{GW},\sigma}(\epsilon_m^\sigma) | \varphi_m^\sigma \rangle], \end{aligned} \quad (19)$$

where ϵ_m^σ and φ_m^σ are qs*GW* QP energies and wavefunctions, respectively. Eq. (19) is referred to as the quasiparticle self-consistent approximation in this work. When $\Sigma_c^\sigma = \Sigma_c^{\text{qsGW},\sigma}$ in Eq. (6), Eq. (4) becomes the qs*GW* QP equation, which updates both eigenvalues and eigenvectors and thus gives both QP energies and wavefunctions.⁴⁴

It should be noted that for the construction of the $\Sigma_c^{\text{qsGW},\sigma}$ matrix in Eq. (19), plane wave-based MBPT codes use truncated basis sets for efficiency, whereas Gaussian-based MOLGW uses all basis sets, because Gaussian basis sets are much more compact than plane wave ones.^{10,44}

D. Second-order Møller–Plesset perturbation theory (MP2)

MP2 is the second-order expansion of the self-energy in v and is the simplest post-HF method. For molecules with weak screening, v is close to W , so MP2 and *GW* methods give similar results for the IE of atoms and molecules.^{38,43} The correlation part of the MP2 self-

energy $\Sigma_c^{\text{MP2},\sigma}(\omega)$ is given by³⁸

$$\begin{aligned}
& \langle \varphi_m^\sigma | \Sigma_c^{\text{MP2},\sigma}(\omega) | \varphi_n^\sigma \rangle \\
&= \sum_{iap\sigma'} (mp\sigma | ia\sigma') (pn\sigma | ai\sigma') \\
&\times \left[\frac{f_p^\sigma}{\omega + \epsilon_a^{\sigma'} - \epsilon_i^{\sigma'} - \epsilon_p^\sigma - i\eta} + \frac{1 - f_p^\sigma}{\omega + \epsilon_i^{\sigma'} - \epsilon_a^{\sigma'} - \epsilon_p^\sigma + i\eta} \right] \\
&- \sum_{iap} (mp\sigma | ia\sigma) (pi\sigma | an\sigma) \\
&\times \left[\frac{f_p^\sigma}{\omega + \epsilon_a^\sigma - \epsilon_i^\sigma - \epsilon_p^\sigma - i\eta} + \frac{1 - f_p^\sigma}{\omega + \epsilon_i^\sigma - \epsilon_a^\sigma - \epsilon_p^\sigma + i\eta} \right], \tag{20}
\end{aligned}$$

where i runs over occupied states, a runs over empty states, p runs over both occupied and empty states, and ϵ_m^σ and φ_m^σ are HF energies and wavefunctions, respectively. On the right side of Eq. (20), the first summation is the second-order Coulomb (direct) interaction, and the second summation is the second-order exchange (SOX) interaction. Like the G_0W_0 method, the one-shot MP2 method starting from HF (MP2@HF) uses only diagonal elements ($m = n$) of Eq. (20), giving only QP energies.

The quasiparticle self-consistent MP2 (qsMP2) method is a MP2 counterpart of the qsGW method. For molecules with strong correlation, qsMP2 gives more stable results than MP2@HF.⁵ Applying the quasiparticle self-consistent approximation in Eq. (19) to $\Sigma_c^{\text{MP2},\sigma}(\omega)$ in Eq. (20) gives the correlation part of the qsMP2 self-energy $\Sigma_c^{\text{qsMP2},\sigma}$:

$$\begin{aligned}
& \langle \varphi_m^\sigma | \Sigma_c^{\text{qsMP2},\sigma} | \varphi_n^\sigma \rangle \\
&= \frac{1}{2} [\langle \varphi_m^\sigma | \Sigma_c^{\text{MP2},\sigma}(\epsilon_n^\sigma) | \varphi_n^\sigma \rangle + \langle \varphi_n^\sigma | \Sigma_c^{\text{MP2},\sigma}(\epsilon_m^\sigma) | \varphi_m^\sigma \rangle], \tag{21}
\end{aligned}$$

where ϵ_m^σ and φ_m^σ are qsMP2 QP energies and wavefunctions, respectively. When $\Sigma_c^\sigma = \Sigma_c^{\text{qsMP2},\sigma}$ in Eq. (6), Eq. (4) becomes the qsMP2 QP equation.

It should be noted that the correlation part of the MP2 self-energy in Eq. (20) is different from the MP2 correlation energy. The MP2 self-energy is for excited-state properties, such as electron attachment and detachment energies, whereas the MP2 correlation energy is for ground-state properties, such as total energy. For atoms and molecules, the so-called Δ SCF method based on the MP2 total energy gives similar vertical IEs to the MP2 self-energy method.³⁸

E. Computational costs of qsGW and qsMP2

In terms of *compute time*, qsGW and qsMP2 methods are computationally much more demanding than one-shot G_0W_0 and MP2@HF methods because of a couple of reasons. First, one-shot G_0W_0 and MP2@HF methods need no SCF iteration, but qsGW and qsMP2 methods

require dozens of SCF iterations.^{7,45} Second, while one-shot G_0W_0 and MP2@HF methods need to calculate only diagonal ($m = n$) elements of the $\langle \varphi_m | \Sigma_c(\omega) | \varphi_n \rangle$ matrix in Eqs. (17) and (20), qsGW and qsMP2 methods have to calculate all elements. Last, whereas one-shot G_0W_0 and MP2@HF methods need to solve QP equations for a couple of MOs of interest, such as frontier MOs, qsGW and qsMP2 methods have to solve QP equations for all MOs.

However, qsGW and qsMP2 methods use almost the same amount of *memory* as one-shot G_0W_0 and MP2@HF methods, and thus are ideal for GPU acceleration. Memory-hungry electronic-structure methods that demand a large amount of memory are not suitable for GPU computing, because they cannot run on the GPU with a small memory.

F. Computational bottlenecks

Figure 1 depicts a flowchart of qsGW and qsMP2 implementations in MOLGW. Figure 1 shows the computational bottlenecks, such as J in Eq. (7), K in Eq. (10), the AO-MO integral transformation in Eq. (16), Σ_c^{qsGW} in Eqs. (17), (18), and (19), and Σ_c^{qsMP2} in Eqs. (20) and (21). For the AO-MO integral transformation in Eq. (16), the compute time scales as $O(N^5)$ with N being the system size, because MOLGW uses a traditional implementation that reduces the $O(N^8)$ algorithm to $O(N^5)$.⁴⁶ The AO-MO integral transformation is a major computational bottleneck common in qsGW and qsMP2 calculations, as shown in Eqs. (16), (17), (18), and (20). For the Casida matrix in Eqs. (12), (13), and (14), the construction time and memory scale as $O(N^5)$ and $O(N^4)$, respectively, and the diagonalization time scales as $O(N^6)$. In this work, the construction and diagonalization of the Casida matrix are minor computational bottlenecks, because small Casida matrices are used.

III. IMPLEMENTATION DETAILS

A. OpenACC implementation

OpenMP and OpenACC are multi-platform shared-memory (thread-based) parallel programming models, which can target both CPUs and GPUs and are free from the inter-process communication overhead in distributed-memory (process-based) models such as MPI, as discussed in Section II B.^{7,28,47} Although OpenMP supports GPU offloading,⁴⁸ we used OpenMP for CPUs and OpenACC for GPUs in this work, because for now OpenACC is a more mature model for GPU offloading than OpenMP.

Table I summarizes OpenACC directives and clauses used in this work and presents where and why they are

```

1 ! Program: MOLGW
2 ! File: pt2_selfenergy.f90
3 ! Description: Calculate the correlation part of the qsMP2 self-energy
4 ! Author1: Fabien Bruneval (a serial CPU version using Fortran)
5 ! Author2: Young-Moo Byun (a parallel CPU/GPU version using OpenMP/OpenACC)
6
7 subroutine pt2_selfenergy_qs (...)
8   ...
9
10 #if !defined (_OPENMP) && defined (_OPENACC)
11   !$acc data copyin(...) copy(...)
12 #endif
13
14   do pquispin=1,nspin
15     do istate=ncore_G+1,nvirtual_G-1
16       ...
17
18       ! OpenMP/OpenACC-parallelized AO-MO integral transformation
19       call calculate_eri_4center_eigen(...)
20
21       ...
22
23 #if defined (_OPENMP) && !defined (_OPENACC)
24   !$OMP PARALLEL
25   !$OMP DO PRIVATE(...) REDUCTION(+:...) COLLAPSE(2)
26 #endif
27 #if !defined (_OPENMP) && defined (_OPENACC)
28   !$acc parallel loop independent collapse(2)
29 #endif
30
31     do pstate=nsemin,nsemax
32       do qstate=nsemin,nsemax
33         ...
34       enddo
35     enddo
36
37 #if !defined (_OPENMP) && defined (_OPENACC)
38   !$acc end parallel
39 #endif
40 #if defined (_OPENMP) && !defined (_OPENACC)
41   !$OMP END DO
42   !$OMP END PARALLEL
43 #endif
44
45     enddo
46   enddo
47
48 #if !defined (_OPENMP) && defined (_OPENACC)
49   !$acc end data
50 #endif
51
52   ...
53 end subroutine pt2_selfenergy_qs

```

Listing 1. Simplified Fortran source code of the OpenMP- and OpenACC-parallelized subroutine for the calculation of the correlation part of the qsMP2 self-energy

used in the source code. Table I shows that our OpenACC implementation in MOLGW generates a total of 8 kernels for 5 computational bottlenecks and 4 kernels for the AO-MO integral transformation in Eq. (16).

Listing 1 presents an example of OpenMP (CPU) and

OpenACC (GPU) implementations in MOLGW. Listing 1 shows that the calculation of Σ_c^{qsMP2} consists of two computational bottlenecks: the AO-MO integral transformation (a line 19) and Σ_c^{qsMP2} excluding the transformation (lines 31–35) (see Table I). This is the case for the

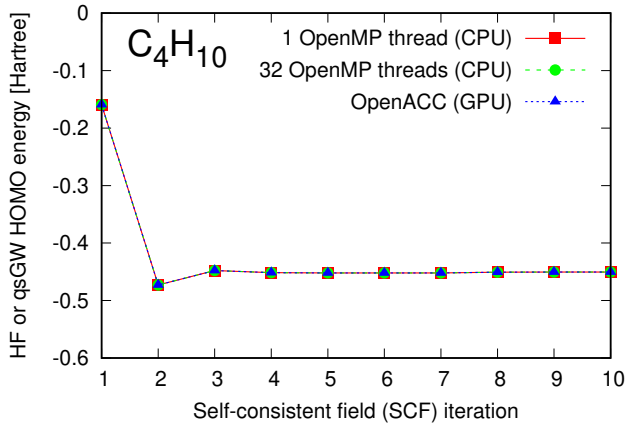


FIG. 2. (Color online) Hartree–Fock (HF) and qsGW energies for the highest occupied molecular orbital (HOMO) of a butane molecule (C_4H_{10}) during the self-consistent field (SCF) iteration, obtained from OpenMP and OpenACC calculations. Total of 10 SCF iterations consist of first 5 HF iterations and subsequent 5 qsGW iterations. The cc-pVTZ basis set is used. $\eta = 0.05$ Hartree in Eq. (17) is used for qsGW. Data is taken from Table II in Supporting Information.

calculation of Σ_c^{qsGW} as well, as shown in Table I. Listing 1 also shows that we did not mix OpenMP (CPU) and OpenACC (GPU) (lines 10, 23, 27, 37, 40, and 48), making the GPU version of MOLGW run on a single CPU core.

We implemented OpenACC into MOLGW 1 and made our local version of MOLGW 1 with OpenMP and OpenACC implementations publicly available via GitHub.⁴⁹ We will merge our OpenACC implementation into MOLGW 3, as the OpenMP implementation was merged into MOLGW 2.⁵

B. Similarities between OpenMP and OpenACC implementations

OpenMP (CPU) and OpenACC (GPU) implementations in MOLGW are similar in a few ways.⁵ First, both annotate the original source code with pragmas without data layout restructuring,⁵⁰ allowing us to preserve the loop order in a serial CPU version, as shown at lines 14, 15, 31, and 32 in Listing 1.

Second, both require code refactoring.⁵¹ For example, we fixed a race condition, which we encountered when parallelizing the implementation of Σ_c^{qsGW} . Also, we changed the index type of some arrays from a 4-byte integer to an 8-byte integer to enable MOLGW to use a large amount of memory. Also, we implemented our own timing routines into MOLGW (for Section V B), because built-in timing routines in MOLGW give wrong results for long calculations.

Third, both parallelize the computational bottlenecks

using similar compiler directives. For example, Listing 1 shows that OpenMP and OpenACC parallelized a loop using `omp parallel do` (lines 24, 25, 41, and 42) and `acc parallel loop` (lines 28 and 38) directives, respectively.

Last, both collapse (merge or unroll) nested loops into a single loop to increase parallelism. For example, Listing 1 shows that OpenMP and OpenACC merged `pstate` and `qstate` loops (lines 31, 32, 34, and 35) using the `collapse` clause (lines 25 and 28, respectively).

C. Differences between OpenMP and OpenACC implementations

However, there are a few differences between OpenMP (CPU) and OpenACC (GPU) implementations in MOLGW. First, unlike OpenMP, OpenACC decouples data movement from computation, as shown at lines 11 and 49 in Listing 1, requiring to optimize the data transfer between host (CPU) and device (GPU) memories after offloading the computation to the GPU. We used CUDA unified (managed) memory, a single memory space for both host and device memories,⁵² to manage dynamically allocated arrays used in the implementation of Σ_c^{qsGW} (see Table I). We used a manual deep copy to handle dynamic data structures, as is done for the OpenACC version of VASP,³⁶ because OpenACC 2.6 does not support a true deep copy (NVIDIA compilers used in this work support the OpenACC 2.6 specification). We transferred global data from CPU memory to GPU memory after the completion of the calculation of the 4-center two-electron Coulomb repulsion integrals in Eq. (8) (see Table I). We used NVIDIA profilers to confirm that we fully optimized the CPU–GPU communication overhead in our OpenACC implementation.

Second, unlike the OpenMP (CPU) implementation, our OpenACC (GPU) implementation does not parallelize the 4-center integrals in Eq. (8), because MOLGW uses Libint, a single instruction multiple data (SIMD)-vectorized CPU library for computing Gaussian integrals.⁵³ The 4-center integrals are calculated only once at the beginning of MOLGW execution, and thus are a major computational bottleneck in non-self-consistent G_0W_0 and MP2@HF calculations, but a minor computational bottleneck in quasiparticle self-consistent GW and MP2 calculations (see Section II E).

Last, the OpenMP (CPU) implementation diagonalizes matrices, such as HF, qsGW, and qsMP2 matrices in Eqs. (4) and (6) with $\Sigma_c^\sigma = 0$, Σ_c^{qsGW} , and Σ_c^{qsMP2} , respectively, and the Casida matrix in Eq. (12) (see Fig. 1), using OpenMP-parallelized Intel math kernel library (MKL), but our OpenACC (GPU) implementation performs the matrix diagonalization serially. In this work, the matrix diagonalization is a minor computational bottleneck, because small matrices are used, as discussed in Section II F.

D. Regression testing

In order to ensure that our parallel GPU version of MOLGW gives the same results as the original serial CPU version, we performed two kinds of regression testing.⁵⁴ First, we used the built-in automated regression test suite in MOLGW and verified that our GPU implementation produces correct results. Second, we compared QP energies obtained from CPU and GPU calculations. Figure 2 depicts HF and qsGW energies for the highest occupied molecular orbital (HOMO) of a butane molecule (C_4H_{10}) from serial CPU, parallel OpenMP CPU, and parallel OpenACC GPU calculations during the SCF iteration, which are presented in Table II in Supporting Information. Figure 2 shows that parallel OpenMP CPU and OpenACC GPU calculations give identical results to the serial CPU calculation, as is the case for qsMP2 as well (see Fig. 1 in Supporting Information). Table II in Supporting Information shows 5 and 10 matching significant digits for HOMO and total energies, respectively, during 10 SCF iterations.

IV. BENCHMARK CONFIGURATIONS

In order to assess the performance of our OpenACC implementation in MOLGW for GPU computing, we conducted a few benchmarks using various software and hardware configurations. We used the following software configurations: First, we used two different starting-point-independent MBPT methods, qsGW and qsMP2, which are computationally the most demanding electronic structure methods in MOLGW. Second, we used the Dunning’s correlation-consistent basis set, cc-pVTZ. Third, we used the first seven linear alkanes (C_nH_{2n+2} , where $n = 1, 2, \dots, 7$) to systemically increase the molecular size and the GPU memory usage. We did not use alkanes larger than heptane (C_7H_{16}) due to our GPU memory limit of 24 GB. To calculate large alkanes, one should reduce the memory usage by using small basis sets, such as cc-pVDZ and Pople’s basis sets, at the cost of accuracy loss or by implementing molecular symmetry into MOLGW. Fourth, for the performance analysis using compute times, we used total of 8 SCF iterations, consisting of first 5 HF iterations [$\Sigma_c = 0$ in Eq. (6)] and subsequent 3 qsGW or qsMP2 iterations [$\Sigma_c = \Sigma_c^{qsGW}$ or Σ_c^{qsMP2} , respectively, in Eq. (6)] (see Fig. 1). It should be noted that dozens of qsGW or qsMP2 iterations are needed to reach the convergence.^{7,45} Fifth, for the roofline performance analysis,⁵⁵ we used total of 6 SCF iterations (1 qsGW or qsMP2 iteration), the Intel Advisor (OpenMP), and the NVIDIA Nsight Compute (OpenACC). Last, we used either Intel or NVIDIA compilers (formerly known as PGI compilers) for OpenMP, but only NVIDIA compilers for OpenACC.

We used the following hardware configurations: For OpenACC, we used two different GPUs, NVIDIA GeForce RTX 3090 and 4090 for a desktop computer (RTX 3090 and RTX 4090, respectively, in the following), whose specifications are summarized in Table II. The RTX 4090 has a newer architecture and higher FP64 performance than the RTX 3090. For OpenMP, we used

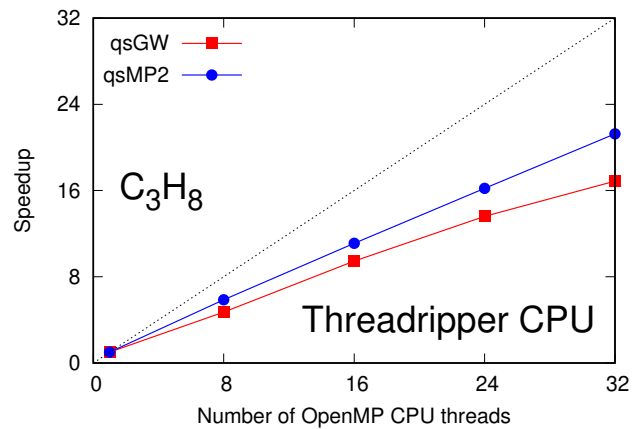


FIG. 3. (Color online) OpenMP speedup as a function of number of CPU threads using different MBPT methods. The cc-pVTZ basis set, the propane molecule (C_3H_8), and the AMD Ryzen Threadripper PRO 3975WX 32-core CPU with 32 SMT disabled are used. *GPUs are not used.* The black dotted line represents the ideal speedup. Data is taken from Table III in Supporting Information.

two different CPUs, AMD Ryzen Threadripper PRO 3975WX with 32 heavyweight cores for a workstation and Intel Xeon Phi 7250 with 68 lightweight cores for a supercomputer (Threadripper and Xeon Phi, respectively, in the following), whose specifications are summarized in Table II. In both Threadripper and Xeon Phi, simultaneous multithreading (SMT), which Intel calls hyper-threading, is disabled. The effect of SMT on the OpenMP (CPU) performance is presented in Table I in Supporting Information.

V. RESULTS AND DISCUSSION

A. Performance analysis using total timings

In order to obtain the GPU speedups over CPU, we performed an OpenMP (CPU) and OpenACC (GPU) benchmark using *total timings* and summarized the benchmark results in Table III. We see a possibility that GPUs can accelerate *large-scale* quasiparticle self-consistent MBPT calculations. For example, the qsGW/cc-pVTZ calculation of the heptane molecule (C_7H_{16}) on the Threadripper and Xeon Phi CPUs using only 3 qsGW iterations takes 15.69 and 23.71 hours of compute time, respectively. The RTX 4090 GPU reduces the compute time to 4.98 hours (by 3.2 and 4.8 times, respectively). As noted in Section IV, about 10 times more iterations and compute times are needed for real calculations.^{7,45} For example, the above calculation on the Xeon Phi CPU using 30 iterations takes about

TABLE II. Specifications for GPUs and CPUs used in this work. GB, (G)DDR, FP64, and GFLOP represent gigabyte, (graphics) double data rate, double-precision floating-point performance, and giga floating-point operations, respectively.

	GPU		CPU	
	RTX 3090 ^a	RTX 4090 ^b	Xeon Phi ^c	Threadripper ^d
Platform	Desktop	Desktop	Supercomputer	Workstation
Release year	2020	2022	2016	2020
Architecture	Ampere	Ada Lovelace	Knights Landing (KNL)	Zen 2 (Castle Peak)
Manufacturing process	8 nm	5 nm	14 nm	7 nm
Number of cores	10496 ^e	16384 ^e	68	32
Boost clock	1.70 GHz	2.52 GHz	1.60 GHz	4.20 GHz
Base clock	1.40 GHz	2.23 GHz	1.40 GHz	3.50 GHz
Memory size	24 GB	24 GB	96 GB	128 GB
Memory type	GDDR6X	GDDR6X	DDR4	DDR4
Memory bandwidth	935.8 GB/s	1008 GB/s	115.2 GB/s	102.4 GB/s ^f
FP64	556 GFLOP/s	1290 GFLOP/s	N/A ^g	268 GFLOP/s ^h

^a NVIDIA GeForce RTX 3090

^b NVIDIA GeForce RTX 4090

^c Intel Xeon Phi 7250

^d AMD Ryzen Threadripper PRO 3975WX

^e Number of compute unified device architecture (CUDA) cores

^f Maximum memory bandwidth for the quad-channel configuration used in this work. The Intel Advisor gives a measured value of 61.2 GB/s.

^g Not available. We can no longer access the Xeon Phi to measure its FP64 using the Intel Advisor, because our supercomputing time grant at the KISTI National Supercomputing Center ended.

^h Measured by the Intel Advisor

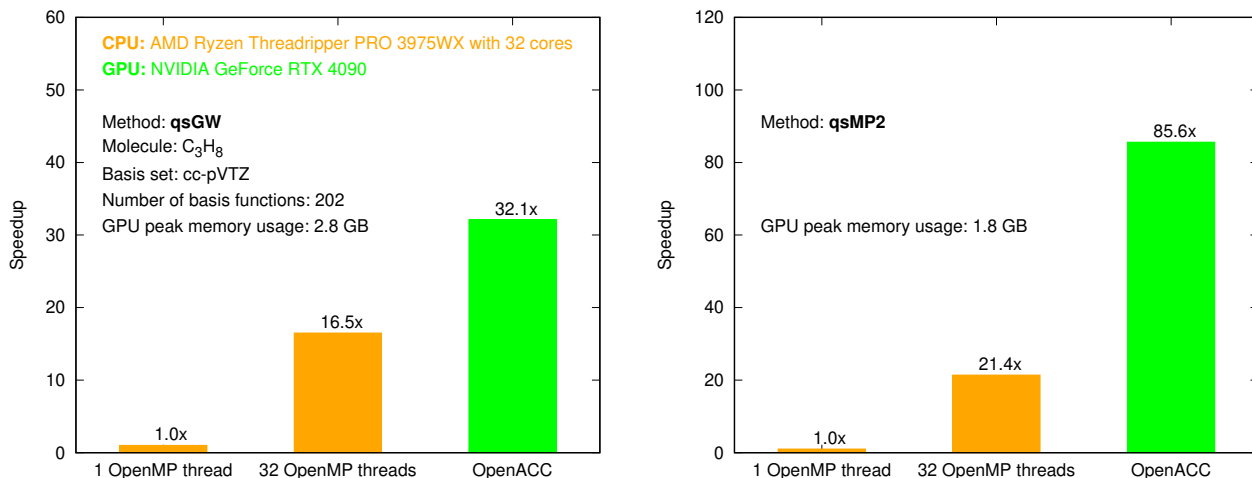


FIG. 4. (Color online) OpenMP and OpenACC speedups of qsGW and qsMP2 methods (left and right, respectively). GB represents gigabyte. Data is taken from Table III.

30 days, which can exceed the walltime limit (typically, about 2 days) in HPC supercomputing centers. In the following, we will visualize and analyze our benchmark results in Table III to find trends.

We begin by briefly checking the OpenMP (CPU) parallel efficiency.⁷ Figure 3 shows the OpenMP speedup as a function of number of CPU threads using different MBPT methods. We used the propane molecule (C₃H₈) and the Threadripper CPU. We see that the qsMP2 method gives a higher parallel efficiency than the qsGW one (~ 0.66

and ~ 0.53 , respectively). This is because the implementation of Σ_c^{MP2} in Eq. (20) takes less steps and thus is simpler than that of Σ_c^{GW} in Eqs. (12), (13), (14), (17), and (18), as shown in Fig. 1. We also see that for both qsGW and qsMP2 methods, the OpenMP parallel efficiency is almost independent of the number of CPU threads (the OpenMP speedup scales nearly linearly with the number of CPU threads).

Next, we compare OpenMP (CPU) and OpenACC (GPU) performances using a single alkane molecule. Fig-

TABLE III. OpenMP and OpenACC compute times using different alkane molecules (C_nH_{2n+2}), MBPT methods, CPUs, and GPUs. GB represents gigabyte.

Molecule	Method ^e	NBF ^f	Memory ^g	OpenMP (hours)			OpenACC (hours)		Speedup	
				Threadripper ^{acj}		Xeon Phi ^{bcdk}	RTX 3090 ^{hj}	RTX 4090 ^{ij}	Threadripper ^l	Xeon Phi ^m
				1 thread	32 threads	68 threads			RTX 4090 ^l	RTX 4090 ^m
CH ₄	qsGW	86	0.1 GB	0.017	0.0014	0.0047	0.0061	0.0031	0.5x	1.5x
C ₂ H ₆	qsGW	144	0.8 GB	0.33	0.018	0.038	0.043	0.018	1.0x	2.1x
C ₃ H ₈	qsGW	202	2.8 GB	2.47	0.15	0.27	0.17	0.077	1.9x	3.5x
C ₄ H ₁₀	qsGW	260	5.0 GB	11.38	0.65	1.00	0.55	0.29	2.2x	3.4x
C ₅ H ₁₂	qsGW	318	9.5 GB	N/A ⁿ	2.65	3.31	1.39	0.87	3.0x	3.8x
C ₆ H ₁₄	qsGW	376	14.9 GB	N/A ⁿ	6.93	9.44	3.03	2.17	3.2x	4.4x
C ₇ H ₁₆	qsGW	434	21.6 GB ^o	N/A ⁿ	15.69	23.71	6.80	4.98	3.2x	4.8x
CH ₄	qsMP2	86	0.1 GB	0.11	0.0056	0.012	0.0078	0.0039	1.4x	3.1x
C ₂ H ₆	qsMP2	144	0.5 GB	1.69	0.081	0.16	0.056	0.029	2.8x	5.5x
C ₃ H ₈	qsMP2	202	1.8 GB	9.42	0.44	0.92	0.26	0.11	4.0x	8.4x
C ₄ H ₁₀	qsMP2	260	4.4 GB	31.48	1.69	3.46	0.82	0.34	5.0x	10.2x
C ₅ H ₁₂	qsMP2	318	8.6 GB	N/A ⁿ	6.06	9.09	1.94	0.81	7.5x	11.2x
C ₆ H ₁₄	qsMP2	376	14.5 GB	N/A ⁿ	14.96	21.94	4.12	1.68	8.9x	13.1x
C ₇ H ₁₆	qsMP2	434	21.4 GB ^o	N/A ⁿ	29.88	45.40	7.89	3.08	9.7x	14.7x

^a AMD Ryzen Threadripper PRO 3975WX 32-core CPU

^b Intel Xeon Phi 7250 68-core CPU

^c Simultaneous multithreading (SMT) is disabled.

^d Single-thread calculations are not performed on the Xeon Phi CPU, which is made up of lightweight cores with a base clock of 1.40 GHz, as shown in Table II.

^e Only 3 qsGW and qsMP2 iterations are used for benchmark purposes. For real calculations, one should use about 10 times more iterations, leading to about 10 times larger OpenMP and OpenACC compute times.

^f NBF represents the number of basis functions. The cc-pVTZ basis set is used.

^g GPU peak memory usage

^h NVIDIA GeForce RTX 3090 GPU on a desktop computer with the AMD Ryzen 9 3950X 16-core CPU

ⁱ NVIDIA GeForce RTX 4090 GPU on a desktop computer with the AMD Ryzen 9 5950X 16-core CPU

^j NVIDIA compilers (formerly known as PGI compilers) are used.

^k Intel compilers are used.

^l OpenMP time from the Threadripper CPU using 32 threads over OpenACC time from the RTX 4090 GPU

^m OpenMP time from the Xeon Phi CPU using 68 threads over OpenACC time from the RTX 4090 GPU

ⁿ Not available because single-thread calculations are prohibitively expensive.

^o qsGW and qsMP2 calculations of alkanes larger than C₇H₁₆ are not performed on GPUs, because those calculations require more memory than available on the RTX 3090 and 4090 GPUs (24 GB, as shown in Table II).

ure 4 shows OpenMP and OpenACC speedups of different MBPT methods. We used the propane molecule (C₃H₈), the Threadripper CPU, and the RTX 4090 GPU. We see a couple of trends. First, for both qsGW and qsMP2 methods, OpenACC achieves higher speedups than 32 OpenMP threads (by 1.9x and 4.0x, respectively), which shows that GPUs can perform high-precision MBPT calculations of molecules faster than CPUs. Second, for both OpenMP and OpenACC, the qsMP2 method gets higher speedups than the qsGW one (by 1.3x and 2.7x, respectively), which shows that the performance boost from parallelization depends on the kind of MBPT methods.

Finally, we analyze the effect of the molecule size on the OpenACC (GPU) performance. Figure 5 shows the OpenACC GPU speedup with respect to OpenMP CPU threads as a function of alkane (C_nH_{2n+2}) size using different MBPT methods, GPUs, and CPUs. We see a few trends. First, the OpenACC speedup depends on the

kind of MBPT methods: for all alkane sizes and GPUs, the qsMP2 method gets higher OpenACC speedups than the qsGW one. This trend will be discussed in detail in Section V B.

Second, the OpenACC speedup increases with the alkane size (the basis size or the GPU memory footprint):^{23,48} for all MBPT methods and GPUs, larger alkane molecules get higher OpenACC speedups, because large arrays utilize more CUDA cores than small arrays. For example, qsGW calculations of butane and heptane molecules (C₄H₁₀ and C₇H₁₆, respectively) on the RTX 4090 GPU use 5.0 and 21.6 GB of GPU memory, respectively, and get OpenACC speedups of 2.2x and 3.2x, respectively, compared to those on the Threadripper CPU, as shown in Table III. Also, *small-scale* MBPT calculations using small basis sets might not benefit from GPU acceleration, because they do not have a sufficient number of threads to saturate CUDA cores. For example, the qsGW calculation of the methane molecule (CH₄),

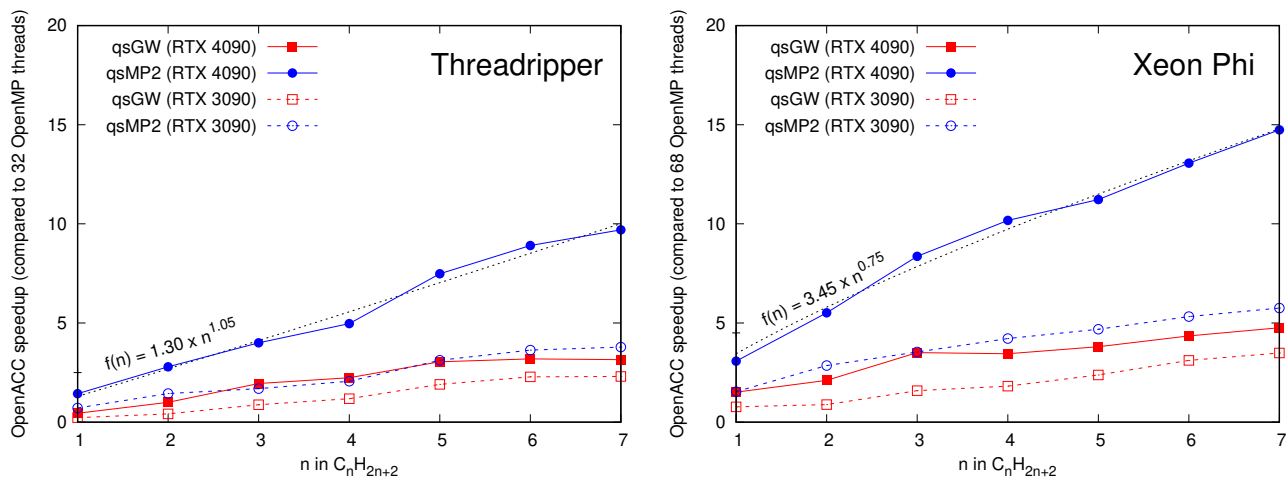


FIG. 5. (Color online) OpenACC GPU speedup relative to OpenMP CPU threads as a function of alkane (C_nH_{2n+2}) size using different MBPT methods and GPUs. The Threadripper 32-core and Xeon Phi 68-core CPUs (left and right, respectively) with SMT disabled are used. The cc-pVTZ basis set is used. The black dotted line is a fitted line for the qsMP2 method on the RTX 4090 GPU. Data is taken from Table III.

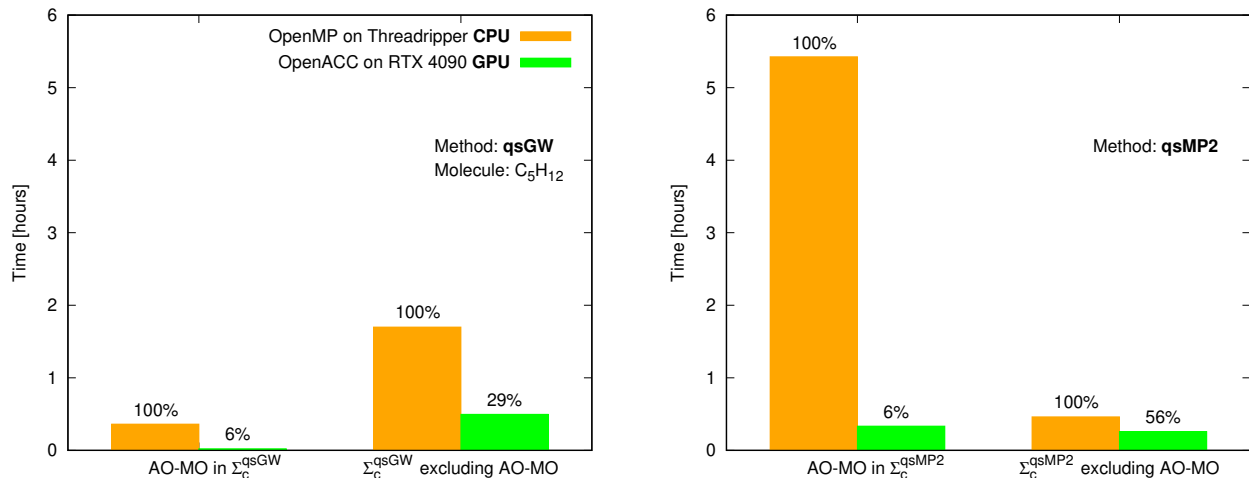


FIG. 6. (Color online) Decomposed OpenMP and OpenACC compute times of Σ_c^{qsGW} and Σ_c^{qsMP2} calculations (left and right, respectively) of the pentane molecule (C_5H_{12}). The Threadripper CPU and the RTX 4090 GPU are used for OpenMP and OpenACC, respectively. The cc-pVTZ basis set is used. AO-MO represents the atomic orbital-to-molecular orbital integral transformation. Data is taken from Tables IV and V in Supporting Information.

the smallest alkane, on the RTX 4090 GPU uses only 86 basis functions and gets an OpenACC speedup of 0.5x relative to that on the Threadripper CPU (the calculation runs faster on the CPU than on the GPU), as shown in Table III. This trend will be discussed in detail in Section V C.

We analyzed the asymptotic time complexity of the OpenACC speedup with respect to alkane (C_nH_{2n+2}) size using a fitting function:

$$f(n) = \alpha \times n^\beta, \quad (22)$$

where α and β are fitting constants, and summarized the analysis results in Table VI in Supporting Information. For example, we obtained $f(n) = 1.30 \times n^{1.05}$ for the

qsMP2 method on the RTX 4090 GPU and the Threadripper CPU, as shown in Fig. 5. The scaling factor β ranges from 0.56 (the qsGW method on the RTX 4090 GPU and the Xeon Phi CPU) to 1.21 (the qsGW method on the RTX 3090 GPU and the Threadripper CPU).

Third, the OpenACC speedup depends on the kind of CPUs: for all MBPT methods and alkane sizes, the Xeon Phi CPU underperforms the Threadripper CPU, taking longer OpenMP compute times and thus giving higher OpenACC speedups. For example, for the qsMP2 calculation of C_4H_{10} , the Xeon Phi CPU gives a 2.0x higher OpenACC speedup than the Threadripper CPU, as shown in Table III.

Last, the OpenACC speedup increases with the GPU

TABLE IV. Dynamic random access memory (DRAM) arithmetic intensity (AI) and double-precision floating-point performance (FP64) of major computational bottlenecks in qsGW and qsMP2 calculations of alkane molecules (C_nH_{2n+2}), obtained from the NVIDIA Nsight Compute. (G)FLOP represents (giga) floating-point operations. AO-MO represents the atomic orbital-to-molecular orbital integral transformation. Σ_c^{qsGW} and Σ_c^{qsMP2} represent the correlation part of qsGW and qsMP2 self-energies, respectively.

Molecule ^a	OpenACC (FLOP/byte for AI and GFLOP/sec for FP64)											
	NVIDIA GeForce RTX 4090 GPU											
	AO-MO								Σ_c^{qsGW} excl. AO-MO	Σ_c^{qsMP2} excl. AO-MO	AI	FP64
	1st kernel		2nd kernel		3rd kernel		4th kernel					
AI	FP64	AI	FP64	AI	FP64	AI	FP64	AI	FP64	AI	FP64	
CH ₄	1.78	22.45	35.76	135.3	36.84	120.2	36.59	129.8	0.25	17.36	4230	317.5
C ₂ H ₆	0.18	32.24	51.44	162.5	50.56	147.6	50.89	162.1	0.13	28.28	9840	466.6
C ₃ H ₈	0.13	33.44	42.04	210.1	41.34	188.0	32.91	144.7	0.07	12.54	13714	613.0
C ₄ H ₁₀	0.11	31.51	44.59	234.8	44.40	211.3	0.70	103.1	0.04	7.39	18102	604.8
C ₅ H ₁₂	0.12	33.11	49.41	277.4	49.89	239.2	0.34	81.1	0.03	6.56	21569	651.8
C ₆ H ₁₄	0.14	37.42	56.69	319.5	56.29	243.2	0.32	70.3	0.03	6.37	24942	705.3
C ₇ H ₁₆	N/A ^b	N/A ^b	N/A ^b	N/A ^b	N/A ^b	N/A ^b	N/A ^b	N/A ^b	N/A ^b	N/A ^b	N/A ^b	N/A ^b

^a See Table III for the number of basis functions and the GPU peak memory usage

^b Not available because profiling calculations are prohibitively expensive. Profiling calculations take more than 10 times longer than normal calculations.

TABLE V. GPU utilization of major computational bottlenecks in qsGW and qsMP2 calculations of alkane molecules (C_nH_{2n+2}), obtained from the NVIDIA Nsight Compute. AO-MO represents the atomic orbital-to-molecular orbital integral transformation. Σ_c^{qsGW} and Σ_c^{qsMP2} represent the correlation part of qsGW and qsMP2 self-energies, respectively.

Molecule ^a	OpenACC (%)											
	NVIDIA GeForce RTX 4090 GPU											
	AO-MO								Σ_c^{qsGW} excl. AO-MO	Σ_c^{qsMP2} excl. AO-MO	Memory	Compute
	1st kernel		2nd kernel		3rd kernel		4th kernel					
Memory	Compute	Memory	Compute	Memory	Compute	Memory	Compute	Memory	Compute	Memory	Compute	
CH ₄	19.2	7.3	33.0	81.1	28.7	69.8	31.4	76.4	33.1	1.6	1.4	38.2
C ₂ H ₆	29.8	10.5	30.9	79.4	38.9	66.2	62.6	72.9	75.9	2.5	2.6	55.9
C ₃ H ₈	35.6	10.8	31.0	79.8	28.9	69.3	74.4	53.3	33.6	1.1	3.8	73.4
C ₄ H ₁₀	37.2	9.9	30.4	81.2	64.0	67.6	57.1	33.0	19.8	0.7	3.7	72.4
C ₅ H ₁₂	41.1	10.1	30.5	81.4	70.7	66.6	48.7	22.5	20.0	0.6	3.9	77.9
C ₆ H ₁₄	42.8	11.1	30.5	81.4	93.5	61.9	42.1	17.9	20.1	0.6	4.4	84.3
C ₇ H ₁₆	N/A ^b	N/A ^b	N/A ^b	N/A ^b	N/A ^b	N/A ^b	N/A ^b	N/A ^b	N/A ^b	N/A ^b	N/A ^b	N/A ^b

^a See Table III for the number of basis functions and the GPU peak memory usage

^b Not available because profiling calculations are prohibitively expensive. Profiling calculations take more than 10 times longer than normal calculations.

generation: for all MBPT methods and alkane sizes, the RTX 4090 GPU takes shorter OpenACC compute times and thus gives higher OpenACC speedups than the RTX 3090 GPU (see Table II for their specifications). For example, for qsGW and qsMP2 calculations of C₄H₁₀, the RTX 4090 GPU gives higher OpenACC speedups than the RTX 3090 GPU by 1.9 and 2.4 times, respectively, as shown in Table III, which are close to the ratio of the RTX 4090 FP64 performance to the RTX 3090 one (1290 GFLOP/s \div 556 GFLOP/s \approx 2.3), as shown in Table II.

Overall, the qsMP2 calculation of C₇H₁₆ on the RTX 4090 GPU using 21.4 GB of GPU memory achieves the

highest OpenACC speedup of 9.7x and 14.7x with respect to that on the Threadripper and Xeon Phi CPUs, respectively, as shown in Table III. Based on the trends above, we expect that larger-memory-footprint MBPT calculations on high-end GPUs, such as the NVIDIA H100 with a high FP64 performance and 80 GB of an extension of the second generation of high bandwidth memory (HBM2e), would achieve higher OpenACC speedups than 9.7x and 14.7x.

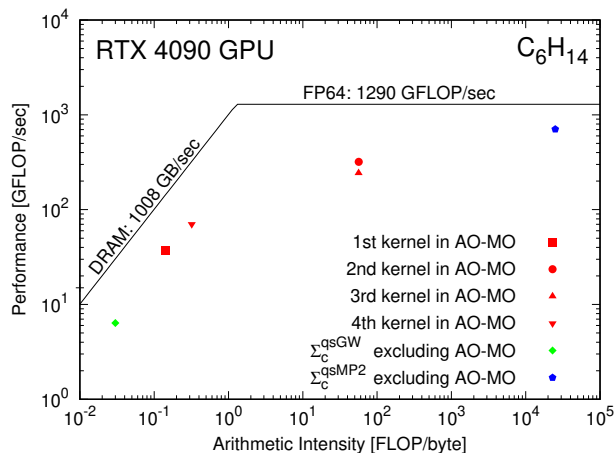


FIG. 7. (Color online) Roofline analysis of Σ_c^{qsGW} and Σ_c^{qsMP2} calculations of the hexane molecule (C_6H_{14}) on the NVIDIA GeForce RTX 4090 GPU, obtained from the NVIDIA Nsight Compute. AO-MO represents the atomic orbital-to-molecular orbital integral transformation. (G)FLOP and GB represent (giga) floating-point operations and gigabyte, respectively. DRAM and FP64 represent dynamic random access memory bandwidth and double-precision floating-point performance, respectively. Data is taken from Tables II and IV.

B. Performance analysis using partial timings

In order to find why the qsMP2 method gets higher OpenACC speedups than the qsGW method, as seen in Section V A, we performed an OpenMP (CPU) and OpenACC (GPU) benchmark using *partial timings* and summarized the benchmark results in Tables IV and V in Supporting Information. As explained in Section III A, the Σ_c^{qsMP2} calculation is composed of two computational bottlenecks: the AO-MO integral transformation (AO-MO in the following) and the AO-MO-excluded Σ_c^{qsMP2} (see Table I and Listing 1), which is the case for the Σ_c^{qsGW} calculation as well. Figure 6 shows decomposed OpenMP (CPU) and OpenACC (GPU) compute times of Σ_c^{qsGW} and Σ_c^{qsMP2} calculations of the pentane molecule (C_5H_{12}) on the Threadripper CPU and the RTX 4090 GPU. We see that in the case of OpenMP (CPU) calculations, the AO-MO bottleneck does not dominate the Σ_c^{qsGW} calculation, but does the Σ_c^{qsMP2} calculation. For example, the AO-MO bottleneck takes 4.7 times *less* OpenMP compute time than the AO-MO-excluded Σ_c^{qsGW} bottleneck in the Σ_c^{qsGW} calculation, but 11.8 times *more* OpenMP compute time than the AO-MO-excluded Σ_c^{qsMP2} bottleneck in the Σ_c^{qsMP2} calculation (see Table IV in Supporting Information). We also see that the AO-MO bottleneck benefits the most from GPU acceleration among three major computational bottlenecks. For example, OpenACC (GPU) reduces OpenMP (CPU) compute times of AO-MO, AO-MO-excluded Σ_c^{qsGW} , and AO-MO-excluded Σ_c^{qsMP2} bottlenecks by 94%, 71%, and 46%. As a result, GPU acceleration has a stronger effect on the qsMP2 method than

the qsGW method (GPU speedups of 8.9x and 3.2x, respectively, as shown in Table III).

C. Roofline performance analysis

In order to find what is limiting the performance of our OpenACC implementation, we conducted the roofline performance analysis⁵⁵ of three major computational bottlenecks (a total of 6 kernels) – AO-MO (consisting of 4 kernels), AO-MO-excluded Σ_c^{qsGW} , and AO-MO-excluded Σ_c^{qsMP2} (see Table I) – in OpenACC calculations on the RTX 4090 GPU, and summarized the analysis results in Table IV. Figure 7 depicts the roofline analysis results for the hexane molecule (C_6H_{14}). We see that the AO-MO bottleneck, which is common in qsGW and qsMP2 calculations, has both compute- and memory-bound kernels. For example, the first and fourth kernels in the AO-MO bottleneck are under the peak bandwidth ceiling (diagonal line) and thus are memory-bound, while the second and third kernels are under the peak performance ceiling (horizontal line) and thus are compute-bound. We also see that the AO-MO-excluded Σ_c^{qsGW} bottleneck is highly memory-bound (arithmetic intensity of 0.03 FLOP/byte), whereas the AO-MO-excluded Σ_c^{qsMP2} bottleneck is highly compute-bound (FP64 performance of 705.3 GFLOP/sec) (see Table IV). This shows that the qsGW method is more memory-bound and less compute-bound than the qsMP2 method. We summarized the roofline analysis results for OpenMP calculations on the Threadripper CPU in Table VII in Supporting Information, and depicted the results for C_6H_{14} in Fig. 2 in Supporting Information.

In order to understand the optimization level of our OpenACC implementation, we analyzed the GPU utilization of three major computational bottlenecks (a total of 6 kernels) in OpenACC calculations on the RTX 4090 GPU with the FP64 performance of 1290 GFLOP/s and the memory bandwidth of 1008 GB/s (see Table II), and summarized the analysis results in Table V. We see that the GPU utilization depends on the molecule size. For example, the GPU compute utilization of the AO-MO-excluded Σ_c^{qsMP2} bottleneck increases with the alkane size from 38.2% to 84.3% (CH_4 and C_7H_{16} , respectively), while that of the second kernel in the AO-MO bottleneck remains nearly constant at $\sim 80\%$ across all alkane sizes. Also, the GPU memory utilization of the first kernel in the AO-MO bottleneck increases with the molecule size from 19.2% to 42.8% (CH_4 and C_7H_{16} , respectively), whereas that of the second kernel remains almost unchanged at $\sim 30\%$ across all alkane sizes. We also see that the GPU utilization depends on the kind of kernels. For example, in the case of the hexane molecule (C_6H_{14}), the GPU compute utilization ranges from 0.6% to 84.3% (AO-MO-excluded Σ_c^{qsGW} and Σ_c^{qsMP2} kernels, respectively), and the GPU memory utilization ranges from 4.4% to 93.5% (the AO-MO-excluded Σ_c^{qsMP2} kernel and the third kernel in the AO-MO bottleneck, respectively). We summarized the analysis results for the CPU

utilization of three major computational bottlenecks in OpenMP calculations on the Threadripper CPU with the measured FP64 performance of 268 GFLOP/s and the measured quad-channel memory bandwidth of 61.2 GB/s (see Table II) in Table VIII in Supporting Information.

D. Discussion

We have a few points to discuss. First, OpenMP and OpenACC implementations in MOLGW “added parallelism into existing source code without significantly modifying it,”⁵⁶ enabling us to maintain a *single* version of source code for both CPUs and GPUs. The clean and maintainable MOLGW source code makes it possible for domain scientists, such as electronic structure method developers, with no or little parallel programming background to do “more science and less programming.”⁴⁷

Second, our current OpenACC version of MOLGW runs only on a single GPU. We will enable MOLGW to run on a multi-GPU node using the hybrid OpenMP/OpenACC parallelization in the future. The multi-GPU implementation can enhance scalability of MOLGW,¹⁷ but will reduce readability, understandability, and backward compatibility of source code, because it requires to change the serial CPU code.

Third, the matrix diagonalization in MOLGW is not ported to the GPU, as discussed in Section III C. Although the diagonalization of the Casida matrix scales as $O(N^6)$, it is a minor computational bottleneck in this work due to a small prefactor, as discussed in Section II F. However, it will become a major computational bottleneck in G_0W_0 and qsGW calculations of very large systems. Hence, we will port the matrix diagonalization in MOLGW to the GPU in the future possibly using a GPU-accelerated library for linear algebra.

Last, not all MBPT methods and molecular systems would benefit from GPU acceleration. For example, computationally cheap one-shot G_0W_0 and MP2@HF methods should attain lower GPU speedups than computationally expensive qsGW and qsMP2 ones, as discussed in Section II E. Also, MBPT calculations of small systems could run faster on the CPU than on the GPU, as seen in Section V B, and those of large systems might require more memory than available on the GPU (typically, the CPU has more memory than the GPU, as shown in Table II). Overall, the GPU version of a MBPT code cannot fully replace the CPU version, because CPUs are still needed for certain kinds of MBPT methods and molecular systems.

VI. SUMMARY AND CONCLUSIONS

In summary, we have ported MOLGW to the GPU using OpenACC without sacrificing accuracy, and evaluated the performance of GPU-accelerated MOLGW us-

ing different starting-point-independent MBPT methods, system sizes, and GPUs. We found that the GPU-accelerated version of MOLGW can run faster than the CPU version using 32 OpenMP threads by up to 9.7 times, and the speedup depends on the kind of MBPT methods and increases with the GPU generation and the system size (the basis size or the GPU memory footprint). We identified both compute- and memory-bound kernels in GPU-accelerated MOLGW using the roofline performance analysis. Our choice of OpenACC over CUDA allows us to maintain a single version of the MOLGW source code for both CPUs and GPUs, which significantly reduces programming and maintenance efforts and enhances code and performance portability. Our GPU acceleration of quasiparticle self-consistent MBPT methods in MOLGW paves the way for the application of *ab initio* MBPT calculations without empirical parameters, such as starting points, to complex real systems.

VII. AUTHORSHIP CONTRIBUTION STATEMENT

Young-Moo Byun conceived and designed the project, implemented and validated the computer code, performed the computations, collected the data, analyzed and interpreted the results, and wrote the draft manuscript. Jejoong Yoo supervised the project, provided the computing resources, and reviewed and revised the manuscript. All authors reviewed the results and approved the final version of the manuscript.

VIII. DATA AVAILABILITY STATEMENT

Basis sets and the MOLGW source code with our OpenACC implementation for a single GPU are publicly available via GitHub at <https://github.com/ybyun/molgw-1.F-openmp-openacc-single-gpu>.

ACKNOWLEDGMENTS

This work was supported by the National Research Foundation of Korea (NRF) grant funded by the Korea government (MSIT) (No. 2020R1A2C1101424). This work was supported by Institute for Information & Communications Technology Promotion (IITP) grant funded by the Korea government (MSIT) (No. 2021-0-02068, Artificial Intelligence Innovation Hub). This work was supported by the National Supercomputing Center with supercomputing resources including technical support (KSC-2021-CRE-0212).

* jejoong@skku.edu

¹ G. Onida, L. Reining, and A. Rubio, Rev. Mod. Phys. **74**, 601 (2002).

- ² M. Shishkin and G. Kresse, *Phys. Rev. B* **75**, 235102 (2007).
- ³ M. Govoni and G. Galli, *Journal of Chemical Theory and Computation* **11**, 2680 (2015), pMID: 26575564, <https://doi.org/10.1021/ct500958p>.
- ⁴ M. J. van Setten, F. Caruso, S. Sharifzadeh, X. Ren, M. Scheffler, F. Liu, J. Lischner, L. Lin, J. R. Deslippe, S. G. Louie, C. Yang, F. Weigend, J. B. Neaton, F. Evers, and P. Rinke, *Journal of Chemical Theory and Computation* **11**, 5665 (2015), pMID: 26642984, <https://doi.org/10.1021/acs.jctc.5b00453>.
- ⁵ Y.-M. Byun and S. Ögüt, *The Journal of Chemical Physics* **151**, 134305 (2019), <https://doi.org/10.1063/1.5118671>.
- ⁶ F. Bruneval and M. A. L. Marques, *Journal of Chemical Theory and Computation* **9**, 324 (2013), pMID: 26589035, <https://doi.org/10.1021/ct300835h>.
- ⁷ Y.-M. Byun, J. Yoo, and S. Ögüt, “Practical self-consistent *gw* scheme for electronic structure of open-shell 3d-transition-metal monoxide anions,” To be published elsewhere.
- ⁸ S. V. Faleev, M. van Schilfgaarde, and T. Kotani, *Phys. Rev. Lett.* **93**, 126406 (2004).
- ⁹ M. van Schilfgaarde, T. Kotani, and S. Faleev, *Phys. Rev. Lett.* **96**, 226402 (2006).
- ¹⁰ T. Kotani, M. van Schilfgaarde, and S. V. Faleev, *Phys. Rev. B* **76**, 165106 (2007).
- ¹¹ F. Bruneval and M. Gatti, “Quasiparticle self-consistent *gw* method for the spectral properties of complex materials,” in *First Principles Approaches to Spectroscopic Properties of Complex Materials*, edited by C. Di Valentin, S. Botti, and M. Cococcioni (Springer Berlin Heidelberg, Berlin, Heidelberg, 2014) pp. 99–135.
- ¹² P. Koval, D. Foerster, and D. Sánchez-Portal, *Phys. Rev. B* **89**, 155417 (2014).
- ¹³ F. Kaplan, M. E. Harding, C. Seiler, F. Weigend, F. Evers, and M. J. van Setten, *Journal of Chemical Theory and Computation* **12**, 2528 (2016), pMID: 27168352, <https://doi.org/10.1021/acs.jctc.5b01238>.
- ¹⁴ F. Caruso, M. Dauth, M. J. van Setten, and P. Rinke, *Journal of Chemical Theory and Computation* **12**, 5076 (2016), pMID: 27631585, <https://doi.org/10.1021/acs.jctc.6b00774>.
- ¹⁵ M. J. van Setten, R. Costa, F. Viñes, and F. Illas, *Journal of Chemical Theory and Computation* **14**, 877 (2018), pMID: 29320628, <https://doi.org/10.1021/acs.jctc.7b01192>.
- ¹⁶ M. D. Ben, C. Yang, Z. Li, F. H. d. Jornada, S. G. Louie, and J. Deslippe, in *SC20: International Conference for High Performance Computing, Networking, Storage and Analysis* (2020) pp. 1–11.
- ¹⁷ G. M. J. Barca, M. Alkan, J. L. Galvez-Vallejo, D. L. Poole, A. P. Rendell, and M. S. Gordon, *Journal of Chemical Theory and Computation* **17**, 7486 (2021), pMID: 34780186, <https://doi.org/10.1021/acs.jctc.1c00720>.
- ¹⁸ V. W.-z. Yu and M. Govoni, *Journal of Chemical Theory and Computation* **18**, 4690 (2022), pMID: 35913080, <https://doi.org/10.1021/acs.jctc.2c00241>.
- ¹⁹ P. Needham, A. W. Götz, and R. C. Walker, “Why graphics processing units,” in *Electronic Structure Calculations on Graphics Processing Units* (John Wiley & Sons, Ltd, 2016) Chap. 1, pp. 1–22, <https://onlinelibrary.wiley.com/doi/pdf/10.1002/9781118670712.ch1>.
- ²⁰ P. Needham, A. W. Götz, and R. C. Walker, “Gpus: Hardware to software,” in *Electronic Structure Calculations on Graphics Processing Units* (John Wiley & Sons, Ltd, 2016) Chap. 2, pp. 23–38, <https://onlinelibrary.wiley.com/doi/pdf/10.1002/9781118670712.ch2>.
- ²¹ A. W. Götz, “Overview of electronic structure methods,” in *Electronic Structure Calculations on Graphics Processing Units* (John Wiley & Sons, Ltd, 2016) Chap. 3, pp. 39–66, <https://onlinelibrary.wiley.com/doi/pdf/10.1002/9781118670712.ch3>.
- ²² A. E. I. DePrince and J. R. Hammond, *Journal of Chemical Theory and Computation* **7**, 1287 (2011), pMID: 26610123, <https://doi.org/10.1021/ct100584w>.
- ²³ C. M. Isborn, N. Luehr, I. S. Ufimtsev, and T. J. Martínez, *Journal of Chemical Theory and Computation* **7**, 1814 (2011), pMID: 21687784, <https://doi.org/10.1021/ct200030k>.
- ²⁴ M. S. Gordon, G. Barca, S. S. Leang, D. Poole, A. P. Rendell, J. L. Galvez Vallejo, and B. Westheimer, *The Journal of Physical Chemistry A* **124**, 4557 (2020), pMID: 32379450, <https://doi.org/10.1021/acs.jpca.0c02249>.
- ²⁵ M. S. Gordon and T. L. Windus, *Chemical Reviews* **120**, 9015 (2020), pMID: 32900196, <https://doi.org/10.1021/acs.chemrev.0c00700>.
- ²⁶ J. A. Calvin, C. Peng, V. Rishi, A. Kumar, and E. F. Valeev, *Chemical Reviews* **121**, 1203 (2021), pMID: 33305957, <https://doi.org/10.1021/acs.chemrev.0c00006>.
- ²⁷ “Nvidia cuda homepage,” <https://developer.nvidia.com/cuda-zone>, accessed June 8, 2023.
- ²⁸ “Openacc homepage,” <https://www.openacc.org/> (), accessed June 8, 2023.
- ²⁹ “Dropbox blog,” <https://blog.dropbox.com/topics/company/thank-you--guido>, accessed June 8, 2023.
- ³⁰ J. J. Eriksen, *Molecular Physics* **115**, 2086 (2017), <https://doi.org/10.1080/00268976.2016.1271155>.
- ³¹ D. Bykov and T. Kjaergaard, *Journal of Computational Chemistry* **38**, 228 (2017), <https://onlinelibrary.wiley.com/doi/pdf/10.1002/jcc.24678>.
- ³² V. G. Vergara Larrea, R. D. Budiardja, R. Gayatri, C. Daley, O. Hernandez, and W. Joubert, *Concurrency and Computation: Practice and Experience* **32**, e5780 (2020), <https://onlinelibrary.wiley.com/doi/pdf/10.1002/cpe.5780>.
- ³³ M. Smith, A. Tamerus, and P. Hasnip, *Computing in Science & Engineering* **24**, 46 (2022).
- ³⁴ D.-K. Dang, L. W. Wilson, and P. M. Zimmerman, *Journal of Computational Chemistry* **43**, 1680 (2022), <https://onlinelibrary.wiley.com/doi/pdf/10.1002/jcc.26968>.
- ³⁵ S. Maintz and M. Wetzstein (2018).
- ³⁶ S. Maintz, “Porting vasp to gpus with openacc,” <https://www.nvidia.com/en-us/on-demand/session/gtceurope2018-e8367>, accessed June 8, 2023.
- ³⁷ X. Blase, C. Attaccalite, and V. Olevano, *Phys. Rev. B* **83**, 115103 (2011).
- ³⁸ X. Ren, P. Rinke, V. Blum, J. Wierfink, A. Tkatchenko, A. Sanfilippo, K. Reuter, and M. Scheffler, *New Journal of Physics* **14**, 053020 (2012).
- ³⁹ M. J. van Setten, F. Weigend, and F. Evers, *Journal of Chemical Theory and Computation* **9**, 232 (2013), pMID: 26589026, <https://doi.org/10.1021/ct300648t>.
- ⁴⁰ J. Wilhelm, M. Del Ben, and J. Hutter, *Journal of Chemical Theory and Computation* **12**, 3623 (2016), pMID: 27348184, <https://doi.org/10.1021/acs.jctc.6b00380>.
- ⁴¹ F. Bruneval, T. Rangel, S. M. Hamed, M. Shao, C. Yang, and J. B. Neaton, *Computer Physics Communications*

- 208, 149 (2016).
- ⁴² D. Golze, M. Dvorak, and P. Rinke, *Frontiers in Chemistry* **7**, 377 (2019).
- ⁴³ F. Bruneval, N. Dattani, and M. J. van Setten, *Frontiers in Chemistry* **9** (2021), 10.3389/fchem.2021.749779.
- ⁴⁴ F. Bruneval, N. Vast, and L. Reining, *Phys. Rev. B* **74**, 045102 (2006).
- ⁴⁵ F. Bruneval, *The Journal of Chemical Physics* **136**, 194107 (2012), <https://doi.org/10.1063/1.4718428>.
- ⁴⁶ CrawfordGroup, “C++ programming tutorial in chemistry,” <https://github.com/CrawfordGroup/ProgrammingProjects/>, accessed November 19, 2023.
- ⁴⁷ “Openmp homepage,” <https://www.openmp.org/> (), accessed June 8, 2023.
- ⁴⁸ B. Q. Pham, M. Alkan, and M. S. Gordon, *Journal of Chemical Theory and Computation* **19**, 2213 (2023), pMID: 37011288, <https://doi.org/10.1021/acs.jctc.2c01137>.
- ⁴⁹ Y.-M. Byun, “Molgw 1.f with openmp and openacc (single gpu),” <https://github.com/ybyun/molgw-1.f-openmp-openacc-single-gpu>, accessed June 8, 2023.
- ⁵⁰ C. Bonati, E. Calore, S. Coscetti, M. D’Elia, M. Mesiti, F. Negro, S. F. Schifano, and R. Tripicciono, in *Proceedings of the 2015 International Workshop on Software Engineering for High Performance Computing in Science*, SE4HPCS ’15 (IEEE Press, 2015) p. 9–15.
- ⁵¹ “Code refactoring,” https://en.wikipedia.org/wiki/Code_refactoring, accessed November 28, 2023.
- ⁵² M. Wolfe, “Openacc and cuda unified memory,” <https://www.pgroup.com/blogs/posts/openacc-unified-memory.htm>, accessed June 8, 2023.
- ⁵³ E. F. Valeev, “Libint: A library for the evaluation of molecular integrals of many-body operators over gaussian functions,” <http://libint.valeyev.net/> (2016), version 2.2.0.
- ⁵⁴ “Regression testing,” https://en.wikipedia.org/wiki/Regression_testing, accessed November 28, 2023.
- ⁵⁵ S. Williams, A. Waterman, and D. Patterson, *Commun. ACM* **52**, 65–76 (2009).
- ⁵⁶ J. Yliluoma, “Guide into openmp,” <https://bisqwit.iki.fi/story/howto/openmp/>, accessed June 8, 2023.